

Two-photon production in low-velocity shocks

S. R. KULKARNI¹ AND J. MICHAEL SHULL^{2,3}

¹Owens Valley Radio Observatory 249-17, California Institute of Technology, Pasadena, CA 91125, USA

²CASA, Department of Astrophysical & Planetary Sciences, University of Colorado, Boulder, CO 80303

³Department of Physics & Astronomy, University of North Carolina, Chapel Hill, NC 27599 USA

ABSTRACT

The Galactic interstellar medium abounds in low-velocity shocks with velocities $v_s \lesssim 70 \text{ km s}^{-1}$. Some are descendants of higher velocity shocks, while others start off at low velocity (e.g., stellar bow shocks, intermediate velocity clouds, spiral density waves). Low-velocity shocks cool primarily via Ly α , two-photon continuum, optical recombination lines (e.g., H α), free-bound emission, free-free emission and forbidden lines of metals. The dark far-ultraviolet (FUV) sky, aided by the fact that the two-photon continuum peaks at 1400 Å, makes the FUV band an ideal tracer of low-velocity shocks. Recent *GALEX* FUV images reaffirm this expectation, discovering faint and large interstellar structure in old supernova remnants and thin arcs stretching across the sky. Interstellar bow shocks are expected from fast stars from the Galactic disk passing through the numerous gas clouds in the local interstellar medium within 15 pc of the Sun. Using the best atomic data available to date, we present convenient fitting formulae for yields of Ly α , two-photon continuum and H α for pure hydrogen plasma in the temperature range of 10⁴ K to 10⁵ K. The formulae presented here can be readily incorporated into time-dependent cooling models as well as collisional ionization equilibrium models.

1. MOTIVATION

Supernova remnants and stellar wind bubbles are iconic examples of shocks in the interstellar medium (ISM). These shocks, with the passage of time, descend to lower velocities. Our interest here is shocks with velocities less than 70 km s⁻¹. The post-shock temperature depends on the mean molecular mass, but we adopt a fiducial value of $T_s \leq 10^5 \text{ K}$ and investigate the cooling of such shock-heated hydrogen gas. These shocks cool primarily via Ly α (whose photons are trapped within the shocked region and eventually die on a dust particle) and two-photon continuum. The latter can be detected by Far Ultra-Violet (FUV) imagers. Low-velocity shocks can also arise on Galactic length scales: intermediate-velocity and high-velocity clouds raining down from the lower halo into the disk and gas that is shocked as it enters a spiral arm. Vallée (2017) provides a good description of the Milky Way’s spiral arms, and Kim et al. (2008) discuss Galactic interstellar shocks.

Stellar bow shocks are another major source of low-velocity shocks. For instance, consider our own Sun,

a generic G5V star with a weak stellar wind ($2 \times 10^{-14} M_\odot \text{ yr}^{-1}$) moving into a warm ($\sim 7,000 \text{ K}$) and partially ionized cloud (ionization fraction, $x \approx 1/3$) at a relative speed of 23–26 km s⁻¹ (Frisch et al. 2011; McComas et al. 2012; Zank et al. 2013; Gry & Jenkins 2014). Because this velocity is not larger than the magnetosonic velocity of the interstellar cloud, there is only a “bow wake” instead of a bow shock (McComas et al. 2012). In the Galactic disk, interstellar space is occupied by the Warm Neutral Medium (WNM; 10³ K to 8 × 10³ K), the Warm Ionized Medium (WIM; 8 × 10³ K), and the Hot Ionized Medium (HIM; 10⁵ K to 10⁶ K), in roughly equal proportions.

From studies with SDSS-Apogee + *Gaia*-DR2 (Anguiano et al. 2020), the 3D velocity dispersion of the typical (α -abundance tagged) thin-disk star is 48 km s⁻¹, whereas those belonging to the thick disk have dispersion of 87 km s⁻¹. The majority of these local stars reside in the thin disk with a density ratio $n_{\text{thin}}/n_{\text{thick}} = 2.1 \pm 0.2$. As discussed in a previous study (Shull & Kulkarni 2023), a sizeable number of stars should be moving supersonically through ambient gas in the WNM

and WIM.¹ The sizes of the resulting bow shocks will be determined by the stellar velocity and the magnitude of the stellar wind.

Separately, recent developments warrant a closer look at low-velocity shocks. We draw attention to the discoveries of three large-diameter supernova remnants (Fesen et al. 2021) and a 30-degree long, thin arc in Ursa Major (Bracco et al. 2020). In large part, these findings were made possible with a new diagnostic – *GALEX* FUV continuum imaging. The detection of such faint, extended features demonstrates simultaneously the value of the dark FUV sky (O’Connell 1987) as well as the value of the FUV band in detecting two-photon emission, a distinct diagnostic of warm ($T \lesssim 10^5$ K) shocked gas (Kulkarni 2022).

The primary goal of this paper is to develop accurate hydrogen plasma cooling models, paying attention to the production of the two-photon continuum in warm plasma, $T \lesssim 10^5$ K, the temperature range of interest to low velocity shocks. To this end, we first derive the probability of Ly α , two-photon continuum, and H α resulting from excitation of the ground state of hydrogen to all $n\ell$ levels for $n \leq 5$ (§2). Next, we review rate coefficients for line excitation by collisions with electrons (§3), followed by a review of collisional ionization (§4). The results are combined to construct a cooling curve for warm hydrogen plasma (§5). We then present a comprehensive (isobaric and isochoric) cooling framework and apply it to gas shock heated to 10^5 K (§6). In §7 we summarize our results and discuss future prospects. Unless otherwise stated, the atomic line data (A-coefficients, term values) were obtained from the NIST Atomic Spectra Database² and basic formulae are from Draine (2011).

2. TWO-PHOTON PRODUCTION

Colliding electrons excite hydrogen atoms to various levels and, if sufficiently energetic, ionize H I to H II. Excited levels are also populated by radiative recombination. Excited hydrogen atoms return to the ground state, some by emitting a Lyman-series photon and others via a cascade of optical/IR recombination lines and ending with Ly α emission. Atoms that find themselves in the metastable $2s$ $^2S_{1/2}$ level, if undisturbed over a timescale of $A_{2s \rightarrow 1s}^{-1} \approx 0.12$ s, return to the ground state by emitting a two-photon continuum. Here, $A_{2s \rightarrow 1s}$ is the Einstein A-coefficient for the $2s$ - $1s$ transition (Drake 1986). Its value should be compared to those for allowed transitions (e.g., 6.26×10^8 s⁻¹ for

Table 1. The indexing scheme and spectroscopic terms

i	level	L_k (cm ⁻¹)	k
1	1s	0	-
2	2s	82303	1
3	2p	”	2
4	3s	97544	3
5	3p	”	4
6	3d	”	5
7	4s	102879	6
8	4p	”	7
9	4d	”	8
10	4f	”	9
11	5s	105348	10
12	5p	”	11
13	5d	”	12
14	5f	”	13
15	5g	”	14

NOTE—In constructing this table we follow the notation and term values of Anderson et al. (2000), where i is the index assigned to levels, and k is the index for upper levels excited in transitions from the ground state (1s). The energy for transition k is hcL_k where L_k is the wavenumber (in cm⁻¹). The symbol “” is equivalent to “ditto”. As can be gathered from the entries for L_k , the small differences in energy due to fine structure effects are ignored.

Ly α and $(1-5) \times 10^7$ s⁻¹ for H α , depending on the upper levels, $3s$, $3p$, $3d$, involved.)

The goal of this section is to compute the production of Ly α photons, two-photon continuum and H α resulting from electronic excitation of H atoms. We consider excitations to 15 $n\ell$ levels; see Table 1 for term values and index scheme. We make the following assumptions. (1) The proton density in the plasma is less than the “ $2s$ critical density” of 1.5×10^4 cm⁻³ (see Chapter 14 of Draine 2011). This ensures that atoms in the $2s$ level are not collisionally mixed to the $2p$ level over a timescale of $A_{2s \rightarrow 1s}^{-1}$ and thus relax by emitting a two-photon continuum. (2) The cooling plasma is optically thick to Lyman lines (case B), so that Lyman photons are absorbed in the vicinity of where they are emitted.

¹ Only a few stars are likely transiting the Cold Neutral Medium (CNM; 100 K), given its small volume filling factor, $\sim 1\%$.

² https://physics.nist.gov/PhysRefData/ASD/lines_form.html

Thus, when computing branching ratios, all allowed Lyman series recombinations can be ignored.

2.1. Photon Yields

Consider, for example, an atom excited to one of the $n = 3$ levels. An atom excited to $3s$ or $3d$ will decay to $2p$ by emitting $H\alpha$ followed by $Ly\alpha$. (We ignore forbidden transitions such as $ns-1s$ two-photon decays; see Chluba & Sunyaev 2008.) An atom excited to $3p$ can decay by emitting $Ly\beta$ or decay to $2s$ by emitting $H\alpha$ followed by two-photon decay. For the latter, the branching fraction \mathcal{B}_β for $Ly\beta$ emission is $A_{3p \rightarrow 1s} / (A_{3p \rightarrow 1s} + A_{3p \rightarrow 2s}) \approx 88\%$. However, under case B, the $Ly\beta$ photon will be absorbed elsewhere in the nebula, and the situation will be repeated until de-excitation ends with emission of $H\alpha + Ly\alpha$.

Table 2. Lyman lines: Optical depths and scatterings

line	λ (Å)	f	τ_0	$n\ell$	\mathcal{B}
$Ly\alpha$	1215.67	0.4164	1000	$2p$	1
$Ly\beta$	1025.73	0.07912	160	$3p$	0.881
$Ly\gamma$	972.54	0.02901	56	$4p$	0.839
$Ly\delta$	949.74	0.01394	26	$5p$	0.819

NOTE—Columns 1–4 give the name, wavelength, absorption oscillator strength, and central optical depth of the line. The column density of the nebula is assumed to provide a line-center optical depth of $\tau_0 = 1000$ for $Ly\alpha$, from which τ_0 for other Lyman lines follow. \mathcal{B} (column 6) is the branching ratio for an atom excited to an np level (column 5) to relax by emitting the appropriate Lyman series line, as opposed to a multi-decay cascade.

For a fiducial value of optical depth ($\tau_{0,\alpha} = 1000$) of $Ly\alpha$, Table 2 lists the corresponding optical depths for the Lyman series. The branching ratio \mathcal{B}_γ to emit a $Ly\gamma$ line is slightly smaller than that for $Ly\beta$. As with $Ly\beta$ under case-B conditions, $Ly\gamma$ will also be converted to some combination of $Ly\alpha$, optical/IR recombination lines, and a two-photon continuum. The oscillator strength, $f \propto n^{-3}$, where n is the principal quantum number of the excited state. Thus the Lyman-line optical depths decrease rapidly with increasing n (up the series). In contrast, the branching factors \mathcal{B} decrease slowly with n .

Each state other than $4s$ and $5s$ has two fine-structure levels. For example, the $4p$ state has two levels, $P_{1/2}$ and $P_{3/2}$, with very little energy difference between the

fine structure levels. However, the electron collisional excitation rate coefficients presented below (§3) refer to the sum of transitions to the entire level, e.g., $1s \rightarrow 4p$. The excitation coefficient is divided in proportion to the number of levels of the excited state, $g_u = 2J + 1$ where J is the total angular momentum of the excited state. The photon yields for $Ly\alpha$, 2γ continuum, and $H\alpha$ are given in Table 3.

Table 3. Photon yields for $Ly\alpha$, $H\alpha$, and 2γ continuum

k	$p_k(Ly\alpha)$	$p_k(H\alpha)$	$p_k(2\gamma)$
1	0	0	1
2	1	0	0
3	1	1	0
4	0	1	1
5	1	1	0
6	0.585	0.415	0.415
7	0.261	0.261	0.739
8	0.813	0.187	0.187
9	1	1	0
10	0.513	0.378	0.487
11	0.305	0.265	0.695
12	0.687	0.267	0.313
13	0.936	0.702	0.064
14	1	1	0

NOTE—Photon production yields p_k upon excitation to level with index “ k ”, under case B conditions; see Table 1 for the definition of k . For instance, an H atom excited to $3s$ ($k = 3$) relaxes by emitting one $H\alpha$ photon and one $Ly\alpha$ photon.

3. ELECTRON COLLISIONAL EXCITATION

The excitation of lines of hydrogen due to collisions with electrons is a venerable topic in ISM studies. The classic review by Dalgarno & McCray (1972) summarizes the atomic physics of the 1960s. Scholz & Walters (1991) undertook detailed calculations of the $n = 1 \rightarrow 2$ excitations and also provided an estimate for the cooling rate coefficient, Λ_{HI} . Anderson et al. (2002; see also Anderson et al. 2000) present close-coupling R-matrix calculations. We adopt these rates since they offer improved accuracy over previous studies (Scholz et al. 1990). The Anderson et al. (2002) theoretical cross sections were constructed with 15 physical energy states

Table 4. Polynomial fits to collision strengths^a

k	trans	a_0	a_1	a_2
1	1s-2s	0.5532	0.1044	0.0105
2	1s-2p	5.4261	2.2029	0.2481
3	1s-3s	0.1121	0.0131	0.0008
4	1s-3p	0.9355	0.3518	0.0382
5	1s-3d	0.1957	0.0517	0.0050
6	1s-4s	0.0390	-0.0005	-0.0008
7	1s-4p	0.3224	0.1124	0.0114
8	1s-4d	0.0944	0.0213	0.0016
9	1s-4f	0.0117	0.0011	0.0002
10	1s-5s	0.0175	-0.0019	-0.0004
11	1s-5p	0.1464	0.0501	0.0055
12	1s-5d	0.0471	0.0094	0.0008
13	1s-5f	0.0108	0.0003	-0.0000
14	1s-5g	0.0005	-0.0004	0.0001

^aCoefficients (a_i) for Maxwellian-averaged collision strengths, fitted by $\bar{\Omega}_k = \sum_{i=0}^2 a_i x^i$, where $x = \ln(T/10^6 \text{ K})$. Here, k is the index of the transition (see Table 1).

up to $n = 5$ (1s to 5g) supplemented by 24 pseudo-states described by orbitals $(\bar{n}, \bar{\ell})$ with $\bar{n} = 6 - 9$ and $\bar{\ell} = 0 - 5$.

Anderson et al. (2002) present collision strengths, $\bar{\Omega}_{ij}$, for excitation from levels i to j , averaged over a Maxwellian velocity distribution at electron temperatures, $E_T \equiv k_B T$, ranging from 0.5–25 eV. The collisional excitation rate coefficients (in $\text{cm}^3 \text{ s}^{-1}$) are then given by:

$$q_{i \rightarrow j} = \frac{2\sqrt{\pi} \alpha a_0^2}{g_i} \sqrt{\frac{I_H}{k_B T}} \bar{\Omega}_{ij}(T) \exp(-E_{ij}/kT) \\ = \frac{8.629 \times 10^{-6}}{g_i} \frac{\bar{\Omega}_{ij}}{\sqrt{T}} \exp(-E_{ij}/k_B T), \quad (1)$$

where a_0 is the Bohr radius, α is the fine structure constant, g_i is the degeneracy of level i , and E_{ij} is the energy difference between level i and j . Since we are only interested in excitations from the ground state, we assume $g_i = 2$ for 1s ($^2S_{1/2}$).

Given our focus on warm plasma, we limit the model fits to $1 \text{ eV} \leq E_T \leq 15 \text{ eV}$. After some experimentation, we found that a cubic polynomial provides an adequate fit³:

$$\bar{\Omega}_{ij}(T) = a_1 + a_2 x + a_3 x^2, \quad (2)$$

where $x = \ln(T/10^6 \text{ K})$. The fit is precise to about 1% for all levels except 5 ℓ levels, for which the fitting errors

³ A first-order fit would have been sufficient for excitations to all states but 1s-np and 1s-nd. For simplicity, we elected to use the same number of coefficients for all transitions.

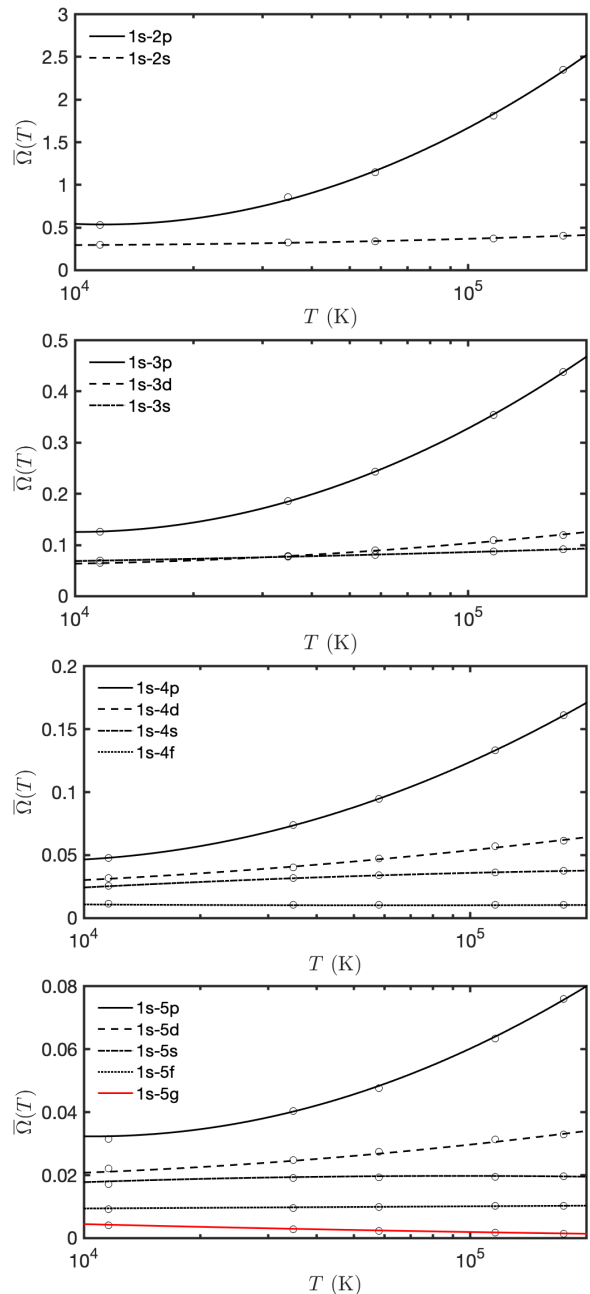


Figure 1. The electron-impact collision strengths, $\bar{\Omega}_{ij}$, for 1s to (n, ℓ) excitations of hydrogen as a function of temperature for $n = 2, 3, 4, 5$. Open circles are model data from Anderson et al. (2002), and the lines are second-order polynomial fits (see Equation 2 and Table 4).

approach 5% (see Figure 1). The fitting coefficients can be found in Table 4.

The line cooling rate per unit volume is given by $n_e n_{\text{HI}} \Lambda_{\text{HI}}$ where $n_e = n_p$ is the electron (and proton) density and n_{HI} is the density of H atoms. The total particle density is $n_t = n_{\text{HI}} + n_e + n_p = n_{\text{H}}(1 + x)$ with $n_{\text{H}} = n_p + n_{\text{HI}}$ and $x = n_e/n_{\text{H}}$.

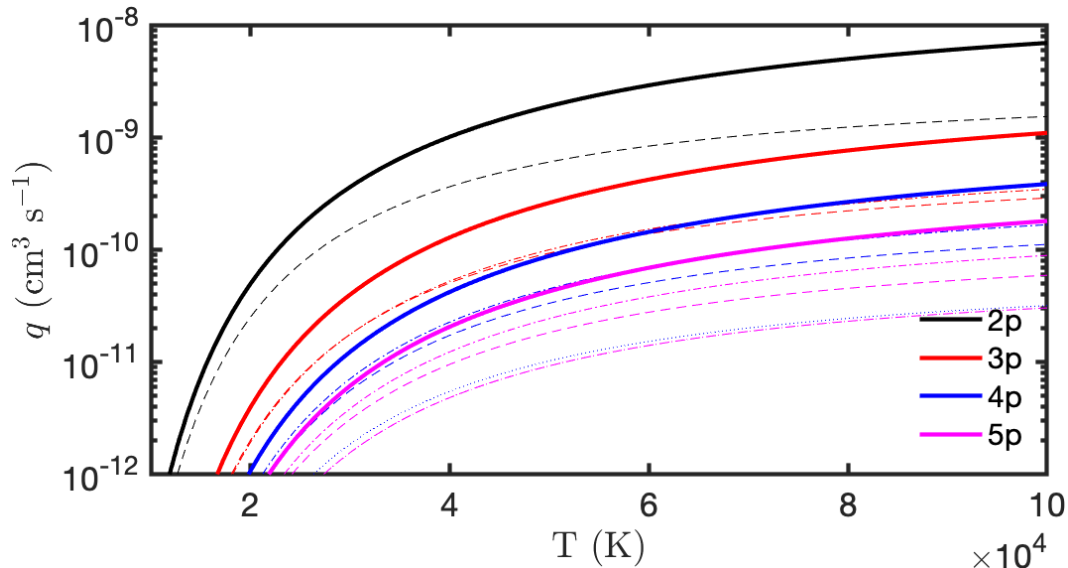


Figure 2. Electron collisional excitation rate coefficients, q_{ij} , for $1s \rightarrow (n, \ell)$ transitions of hydrogen derived from collision strengths provided by Anderson et al. (2002). The curves are coded by color ($n = 2, 3, 4, 5$ as labeled) and by line type (dash-dash $1s$ - ns , continuous for $1s$ - np , dash-dot for $1s$ - nd , dotted for $1s$ - nf , and back to dash-dash for $1s$ - ng .)

We used the fitting model to compute the run of collisional rate coefficients, $q_{i \rightarrow j}$, with temperature (Figure 2). With the cooling coefficients in hand, we computed the sum of the luminosity radiated in lines up to $n = 5$. We consider this sum to be an adequate representation of $\Lambda_{\text{HI}}(T)$ for warm hydrogen. The cooling rate coefficient is

$$\Lambda_{\text{HI}}(T) = \sum_{k=1}^{14} q_k(T) E_k, \quad (3)$$

where the energy of transition with index k is $E_k = hcL_k$; see Table 1 for definition of k and the adopted values for the wavenumbers, L_k (in cm^{-1}). Separately, in §A, we compare this cooling coefficient to previously published coefficients (Spitzer 1978; Scholz & Walters 1991; Dere et al. 1997).

The coefficient for energy loss through line X (where, for instance, X denotes $\text{Ly}\alpha$, $\text{H}\alpha$, 2γ) is given by

$$\Lambda_X(T) = \sum_{k=1}^{14} q_k(T) p_k(X) E_X,$$

where E_X is line energy and $p_k(X)$ is given in Table 3.

3.1. Simple Fits to Line cooling and Collision rates

The collisional excitation rate coefficient is the sum over all hydrogen levels,

$$Q(T) = \sum_{i=1}^{14} q_i(T).$$

Both $Q(T)$ and the hydrogen cooling rate (from excitation to $n = 2$) fall off with temperature as $\exp(-T/T_{12})$, where $k_B T_{12} = 3I_{\text{H}}/4$ is the energy difference between $n = 1$ and $n = 2$ levels. We fit the collision rate and Λ_{HI} over two temperature ranges: “hot” ($10^4 \text{ K} < T < 1.5 \times 10^5 \text{ K}$) and “warm” ($10^4 \text{ K} < T < 1.5 \times 10^4 \text{ K}$),

$$Q_{\text{HI}}(T) = A \exp(-T/T_{12}) \sum_{i=0}^n a_i z^i, \quad (4)$$

where $z = \log T_4$ with $T_4 = (T/10^4 \text{ K})$. A similar expression was derived for $\Lambda_{\text{HI}}(T)$. The fitting parameters for Q_{HI} and Λ_{HI} are given in Table 5, and the quality of the fit is displayed in Figure 3.

Table 5. Fits to Cooling and Collisional Coefficients

Quantity	A	a_0	a_2	a_3	a_4
$\Lambda_{\text{HI}}:\text{hot}$	6.0×10^{-19}	1.018	-0.771	1.537	-0.716
$\Lambda_{\text{HI}}:\text{warm}$	6.0×10^{-19}	1.032	-1.138	3.376	
$Q_{\text{HI}}:\text{hot}$	1.0×10^{-7}	0.371	-0.304	0.560	-0.255
$Q_{\text{HI}}:\text{warm}$	1.0×10^{-7}	0.376	-0.433	1.220	

NOTE—“Quantity” refers to the cooling coefficient (Λ_{HI} in $\text{erg cm}^3 \text{ s}^{-1}$) or collisional excitation rate coefficient (Q_{HI} in $\text{cm}^3 \text{ s}^{-1}$). These quantities are fitted to a model displayed in Equation 4 over two temperature ranges: “hot” ($10^4 \text{ K} < T < 1.5 \times 10^5 \text{ K}$) and “warm” ($10^4 \text{ K} < T < 1.5 \times 10^4 \text{ K}$.)

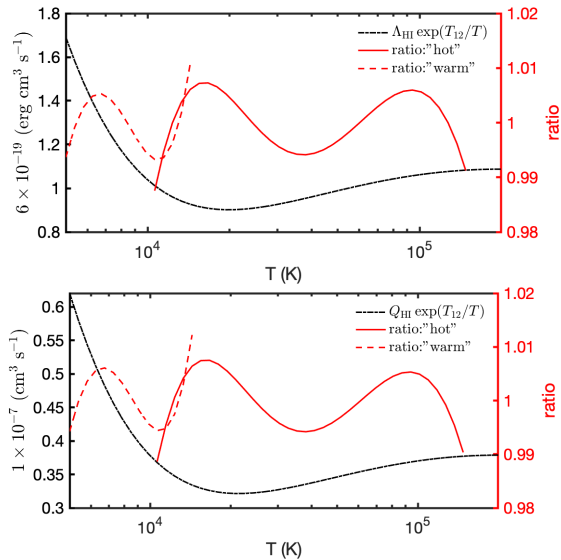


Figure 3. (Top Panel.) Left axis shows the line cooling coefficient, $\Lambda_{\text{HI}}(T)$, for hydrogen (black line), where the total cooling rate is $n_e n_{\text{HI}} \Lambda_{\text{HI}}(T)$. Right axis shows the percent residuals (red-dashed lines) in the form of $[1 - (\Lambda_{\text{HI}}/\text{fit})]$. The model form is given by Equation 4, and model parameters are given in Table 5. (Bottom Panel.) The same, but for Q , the collisional coefficient. The rate of collisions per unit volume is $n_e n_{\text{HI}} Q$.

In Figure 4 we plot the line production efficiency⁴. Consistent with the collisional coefficients displayed in Figure 2 we see that Ly α has the highest efficiency, approximately 2/3, followed by 2-photon emission, 1/3. H α is quite weak, even when measured by photons emitted. H α emission requires excitation to the $n = 3$ level, whereas two-photon and Ly α emission are obtained by excitation to $n = 2$ (and cascade from higher states). However, H α has a major advantage—it can be observed with existing ground-based observatories. For this reason, we provide a fitting formula for $y_{\text{H}\alpha}$, the fraction of H α photons per ionization,

$$f_{\text{H}\alpha} = \sum_{k=0}^2 a_k z^k, \quad (5)$$

where $z = \log T_4$, as before. The model fit for H α is shown in Figure 5, and the values for the model coefficients are given in Table 6, as well as those for Ly α and two-photon emission.

4. ELECTRON COLLISIONAL IONIZATION

⁴ The fraction of photon (e.g. H α , Ly α) emitted per collision. Each two-photon emission is regarded as one event.

Table 6. Efficiency of photon per collision

phot	a_0	a_1	a_2
H α	0.031	0.302	-0.149
2 γ	0.377	-0.095	
Ly α	0.623	0.095	

NOTE— Electron collisions with hydrogen atoms produce Ly α , two-photon continuum (2 γ), H α , and other lines. For each of these categories, the efficiency of photon production, f , depends on temperature and is fitted to a model given by Equation 5. The model fits are accurate to 2%.

The collisional ionization rate coefficient is derived as the integral,

$$k_{ci}(T) = \int_{I_{\text{H}}}^{\infty} \sigma_{ci}(E) v f(E) dE,$$

where $f(E)$ is the Maxwellian energy distribution, $I_{\text{H}} = 13.598$ eV is the ionization energy of hydrogen, and $\sigma_{ci}(E)$ is the collisional ionization cross section as a function of electron energy in the center-of-mass frame, $E = 1/2 \mu v^2$ with $\mu = m_e m_{\text{H}} / (m_e + m_{\text{H}}) \approx m_e$. Here, m_e and m_{H} are the mass of the electron and hydrogen atom, respectively. The collisional ionization rate coefficient can be sensibly written as

$$k_{ci}(T) = A(T) \exp(-I_{\text{H}}/k_B T). \quad (6)$$

Black (1981) provided an approximate form for $k_{ci}(T)$, based on ionization cross sections tabulated by Lotz (1967),

$$k_{ci}(T) = 5.85 \times 10^{-11} T^{1/2} \exp(-I_{\text{H}}/k_B T) \text{ cm}^3 \text{ s}^{-1}. \quad (7)$$

This expression is consistent with the approximation, $\sigma_{ci} \propto (1 - I_{\text{H}}/E)$, quoted in Draine (2011), but only valid at low collision energies ($I_{\text{H}} \leq E \leq 3I_{\text{H}}$). As shown by Lotz (1967), the high-energy behavior is $\sigma_{ci} \propto \ln E/E$. Scholz & Walters (1991) provided a better approximation (for 10^4 K to 2×10^5 K) using a sixth-order polynomial,

$$A(T) = \exp\left(\sum_{i=0}^6 a_i y^i\right) \text{ cm}^3 \text{ s}^{-1} \quad (8)$$

where $y = \ln T$. A comparison (Figure 6) between Equation 7 (Black 1981 fit) and the more accurate Scholz &

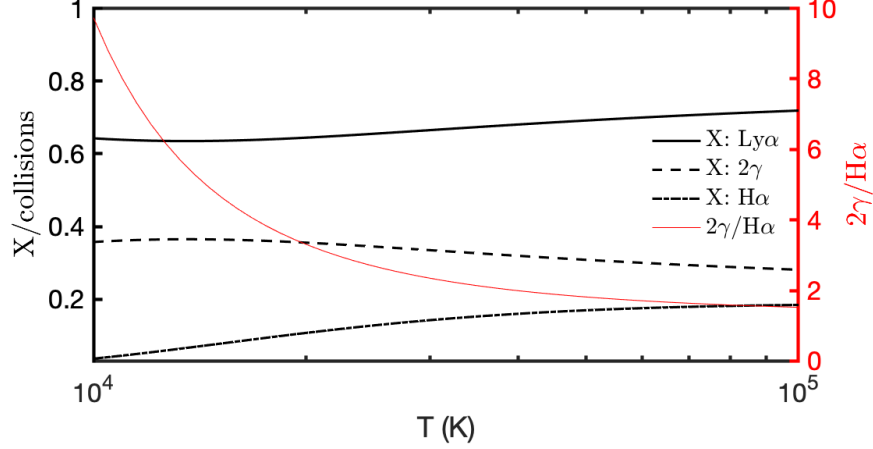


Figure 4. (Left) Case B photon production per collision as a function of temperature, T for $Ly\alpha$, $H\alpha$ and two-photon continuum. (Right) The ratio of yields of two-photon decays to that of $H\alpha$ photons.

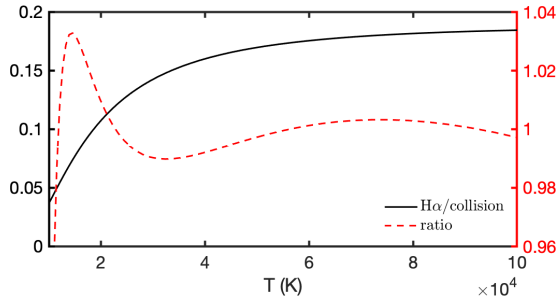


Figure 5. (Left axis) The fraction, $f_{H\alpha}$, of electron collisions with an H I atom that result in emission of an $H\alpha$ photon as a function of temperature. A polynomial model for $y_{H\alpha}$ is described in Equation 5. The ratio of this model to calculations is displayed by the dashed red line.

Walters fit (Equation 8) shows that the former breaks down at high temperatures. We offer a modified formula with the correct asymptotic behavior ($k_B T > I_H$) as used in the shock models of Shull & McKee (1979),

$$k_{ci}(T) = \frac{5.85 \times 10^{-11} T^{1/2}}{[1 + 0.1 k_B T / I_H]} \exp\left(-\frac{I_H}{k_B T}\right) \text{cm}^3 \text{s}^{-1}. \quad (9)$$

As can be seen from Figure 6, this modified formula provides a good fit at both low and high temperatures. For quick estimates we use Equation 9, but the polynomial formulation of Scholz & Walters (1991) is preferred when precision is needed (e.g., in numerical integration of differential equations). The resulting ionization power loss per unit volume is $n_e n_{HI} \Lambda_{ci}$ where $\Lambda_{ci} = k_{ci} I_H$ is the collisional ionization energy loss coefficient.

5. THE HYDROGEN COOLING CURVE

The goal in this section is to construct a cooling curve for “warm” ($T \lesssim 10^5$ K) hydrogen plasma. In §3 we

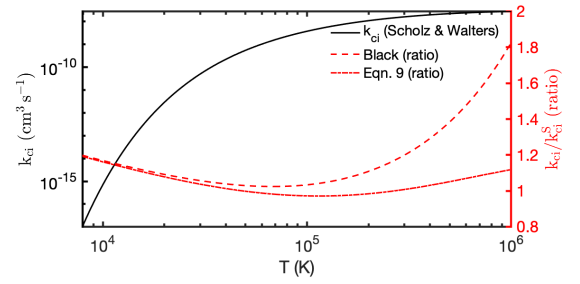


Figure 6. (Left axis): The run of collisional ionization coefficient (black line) of Scholz & Walters (1991). (Right axis): In red, we plot the ratio of the ionization rate coefficients of Black (1981) from Equation 7 and our handy formula (Equation 9) to that of Scholz & Walters (1991) labeled k_{ci}^S .

formulated the cooling coefficient due to line cooling, while in §4 we presented the same for ionization losses. Here, we summarize the cooling coefficients for radiative recombination (free-bound) and free-free losses. Armed thus, we formulate the cooling curve for hydrogen in the temperature range 10^4 K to 10^5 K.

The kinetic energy of recombining electrons is a loss to the thermal pool. The model fits for α_k where $k = 1, A, B$ (corresponding to recombinations to $n = 1s$ level, case A and case B) can be found in Table 7 (§B). The radiative recombination power loss per unit volume is $n_e n_p \alpha \Lambda_{rr}$ where α is either case A or case B, as appropriate. Here, the radiative recombination energy rate coefficient $\Lambda_{rr} = \alpha \langle E_{rr} \rangle$ where $\langle E_{rr} \rangle$ is the mean thermal energy lost by electron upon recombination. Following Draine (2011) we let $\langle E_{rr} \rangle = f_{rr} k_B T$.

The free-free emission rate per unit volume is $n_e n_p \Lambda_{ff}$, where Λ_{ff} is the free-free emissivity. The free-free power per electron is $n_p \Lambda_{ff}$. The mean time for an electron to

recombine is $(n_p\alpha)^{-1}$. Thus, the free-free energy lost up to the point of recombination is $\Lambda_{\text{ff}}/\alpha$, which we equate to $f_{\text{ff}}k_B T$. The combined recombination and free-free cooling rate coefficient is then

$$\Lambda_{\text{rf}} = \Lambda_{\text{rr}} + \Lambda_{\text{ff}} = \alpha f_{\text{rf}}(T)k_B T. \quad (10)$$

where $f_{\text{rf}} = f_{\text{rr}} + f_{\text{ff}}$. The run of $f_{\text{rf}}(T)$ with temperature is displayed in Figure 15 (§B), and the model fits are presented in Table 7 (§B).

We now have all the elements to formulate the cooling rate per unit volume, $\mathcal{C}(T)$, expressed as a negative value (for energy losses):

$$\mathcal{C}(T) = -n_e n_{\text{HI}} [\Lambda_{\text{HI}}(T) + k_{ci}(T)I_{\text{H}}] - n_e n_p \Lambda_{\text{rf}}. \quad (11)$$

The three RHS terms are given by Equations 3, 6, and 10, respectively.

6. LOW-VELOCITY SHOCKS: A SIMPLE COOLING MODEL

The investigation of time-dependent cooling of gas heated to $T \approx 10^5$ K is a classic endeavor, constituting the Ph.D. thesis topics of Michael Jura (Jura & Dalgarno 1972) and Minas Kafatos (Kafatos 1973). The motivation in the 1970s seems to have been ambient gas heated by an FUV shock-breakout pulse. Separately, Draine & Salpeter (1978) investigated the production of Ly α from SN shocks, and Shull & Silk (1979) computed UV emission from SNRs in primeval galaxies.

In unmagnetized plasma, the post-shock temperature of an adiabatic shock is given by

$$T_s = \frac{2(\gamma - 1)}{(\gamma + 1)^2} \frac{\mu v_s^2}{k_B} = (1.12 \times 10^5 \text{ K}) \frac{\mu}{m_{\text{H}}} \left(\frac{v_s}{70 \text{ km s}^{-1}} \right)^2. \quad (12)$$

Here, μ is the mean mass per particle and γ is the ratio of specific heats at constant pressure and constant volume; $\gamma = 5/3$ for mono-atomic gas. If y is the number density of helium relative to that of hydrogen, the mean molecular mass for H^0 and He^0 is $\mu = [(1 + 4y)/(1 + y)]m_{\text{H}} = 1.23m_{\text{H}}$ for $y = 0.0819$ (Planck Collaboration et al. 2020). For H^+ and He^0 , $\mu = 0.64m_{\text{H}}$. For H^+ and He^+ , $\mu = 0.61m_{\text{H}}$, and for H^+ and He^{+2} , $\mu = 0.59m_{\text{H}}$.

Three timescales come into play for post-shocked gas: τ_r , the recombination timescale; τ_{ci} , the collisional ionization timescale; and τ_c , the cooling timescale. For gas around 10^5 K, we have $\tau_{ci} \ll \tau_r$. With this inequality, the cooling gas does not obey the conditions for collisional ionization equilibrium. Thus, it is often essential to undertake a full time-dependent calculation.

6.1. Electron-Proton Equilibration

At the collisionless shock front, the electrons and protons receive similar amounts of random motion. Being more massive, the protons acquire more energy and are initially much hotter than the electrons. The equilibration timescale for electrons to be heated up to the temperature of the protons via electron-proton encounters is approximately

$$t_{\text{loss}} = 14 \left(\frac{T}{10^5 \text{ K}} \right)^{3/2} \left(\frac{\text{cm}^{-3}}{n_e} \right) \left(\frac{25}{\ln\Lambda} \right) \text{ yr},$$

where $\ln\Lambda$ is the Coulomb logarithmic factor accounting for distant encounters (Spitzer 1978; Chapter 2). The current view (Laming et al. 1996; Ghavamian et al. 2007) is that plasma instabilities and electromagnetic waves drive electron-proton equilibration faster than two-body interactions. We assume that equipartition occurs before collisional ionization sets in (§6.2).

6.2. Collisional Ionization

The rate equation for the number density of electrons is

$$\frac{dn_e}{dt} = n_e n_{\text{HI}} k_{ci}(T) - n_e n_p \alpha(T), \quad (13)$$

where $\alpha = \alpha_A, \alpha_B$ as needed. Given our assumption of hydrogen plasma, the number density of protons, $n_p = n_e$. As noted in §C a solution to this equation at constant T is

$$x(t)^{-1} = x_0^{-1} \exp(-t/\tau_{ci}) + x_{eq}^{-1} \left[1 - \exp(-t/\tau_{ci}) \right].$$

Here, $x_0 = x(t=0)$, $\tau_r \equiv (\alpha n_{\text{H}})^{-1}$ and $\tau_{ci} \equiv (k_{ci} n_{\text{H}})^{-1}$ are the characteristic time scales for recombination and collisional ionization, respectively, and

$$x_{eq}(T) = \frac{k_{ci}(T)}{\alpha + k_{ci}(T)} = \frac{\tau_r}{\tau_r + \tau_{ci}}. \quad (14)$$

The lowest probable value for the ionization fraction in a realistic diffuse atomic medium, before heating commences, is $x_0 \approx 2 \times 10^{-4}$. In this case the electrons come from stellar FUV photoionization of C, S, Mg, Si, Fe and other trace metals. The timescale for electron ionization to reach fraction x is $\tau_{ci} \ln(x/x_0)$.

6.3. Recombination

As can be seen from Figure 7, collisional ionization is a strong function of temperature. At late times, when the plasma has cooled, collisional ionization can be ignored and Equation 13 simplifies to $dx/dt = -x^2/\tau_r$, with the solution

$$\frac{1}{x} - \frac{1}{x_0} = \frac{t}{\tau_r}.$$

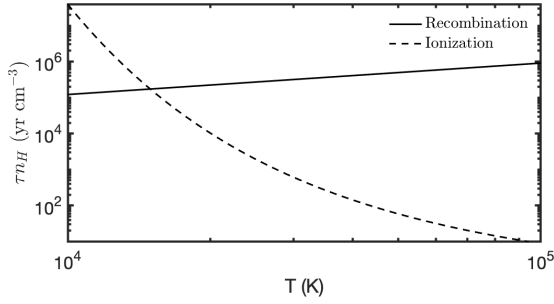


Figure 7. Ionization time (τ_{ci} ; see Equation 9) and recombination time (τ_r ; case B) as a function of temperature. The two timescales cross at about 15,000 K, at which point the ionization fraction would be 50%, if collisional ionization equilibrium were to hold (see Equation 14).

The ionization fraction decreases from x_0 to x_0/m on a timescale of $t = (m - 1)\tau_r/x_0$. The run of recombination time scale as a function of temperature is shown in Figure 7.

6.4. Basic Cooling and Recombining Framework

The path in the phase diagram of density, ionization fraction, and temperature along which the gas cools depends on the circumstances. For planar radiative shocks, the pressure behind the shock is $P_0 + (3/4)\rho_0 v_0^2$, rising to $P_0 + \rho_0 v_0^2$ downstream when $\rho \gg \rho_0$. Here, the pre-shock parameters have subscript 0. Thus, radiative shocks are good examples of cooling at nearly constant pressure (“isobaric”). As the gas cools, its density rises to maintain the pressure. A second possibility is cooling at constant density (“isochoric”). The decrease in temperature, following cooling, leads to lower pressure. Pressure changes are conveyed at the speed of sound, c_s . The time scale for adiabatic sound waves to cross a nebula of length L is $\tau_a = L/c_s$. Isochoric cooling will take place when the cooling time is short, $\tau_c \ll \tau_a$.

The first law of thermodynamics states that any gain in the internal energy (U) of the system is due to increase in internal heat and work done: $dU = dQ - PdV$. For mono-atomic gas, the internal energy of the nebula per unit volume is $U = (3/2)nk_B T$, while the pressure is given by Boyle’s law $P = nk_B T$. Here, $N = nV$ is the total number of particles in the nebula whose volume is V . Let $N_H = n_H V$ be the total number of hydrogen nuclei. Ionization can produce changes in N , whereas N_H is fixed.

The three physical parameters governing the cooling hydrogen plasma are n_e , T and n_H . We have two differential equations, one for ionization balance (n_e ; Equation 13) and one for energy loss (T ; discussed below). A third differential equation follows from the assumed

framework: $dP/dt = 0$ (isobaric cooling) or $dV/dt = 0$ (isochoric cooling).

For an isochoric system, no work is done by or on the nebula. Adopting case B framework the energy balance equations becomes

$$q \frac{d}{dt}(nk_B T) = -n_e n_{HI} [\Lambda_{HI} + k_{ci} I_H] - n_e^2 \alpha_B f_{rf} k_B T,$$

where $q = 3/2$ and the RHS gives the total cooling rate. Note that n_H remains constant, whereas $n = n_H + n_e$ varies as the ionization fraction changes. The ionization-recombination equation (Equation 13) can be restated

$$\frac{dn}{dt} = n_e n_{HI} k_{ci} - n_e^2 \alpha_B.$$

We combine the above two equations to obtain

$$qnk_B \frac{dT}{dt} = -n_e n_{HI} [\Lambda_{HI} + k_{ci} I_H + k_{ci} q k_B T] - n_e^2 \alpha_B (f_{rf} - q) k_B T,$$

which we deliberately recast as

$$qnk_B \frac{dT}{dt} = -n_e n_{HI} [\Lambda_{HI} + k_{ci} I_H] - n_e^2 \alpha_B f_{rf} k_B T + qk_B T [n_e^2 \alpha_B - n_e n_{HI} k_{ci}]. \quad (15)$$

In this formulation, the meaning of Equation 15 is clear. The LHS arises from the loss of internal energy. The first term on the RHS represents energy loss from H I collisional line excitation (Λ_{HI}) and collisional ionization (loss of I_H per collision). The loss of kinetic energy per recombination (including the free-free radiation up until the recombination event) is given by the second term. The final term accounts for losses/gains to the thermal pool of electrons during recombination and ionization. For plasma in collisional ionization equilibrium this term vanishes, as expected.

For isobaric cooling, the pressure, $P = (n_H + n_e)k_B T$ is fixed. In this case, we compute n_e and T and then deduce n_H through the pressure equation. As the nebula cools, the ambient gas, in order to maintain the pressure, P_a , does work on the nebula by compressing the nebula. The work done by the medium on the nebula is PdV . However, since P is constant, $d(PV) = P_a dV$. The internal energy of the nebula is then the enthalpy, HV where $H = U + P_a$. Going forward, we will drop the subscript to P . It is this store of enthalpy that powers the nebular cooling, CV . Since $(U + P)V = (5/2)Nk_B T$ we see that Equation 15 still applies but with $q = 5/2$.

6.5. A shock heated nebula

Consider a nebula composed of hydrogen which has been shocked heated to, say, $T_s = 10^5$ K. The electron-proton equilibration timescale will be shorter than

$14n_e^{-1}$ yr (see §6.1). The collisional ionization time, t_{ci} , is short, $10n_H^{-1}$ yr at $T = 10^5$ K, rising to $60n_H^{-1}$ yr at 50,000 K. Thus, even if the pre-shocked gas has minimal ionization ($x_0 \approx 2 \times 10^{-4}$) it will take a time, $\tau_{ci} \ln(x/x_0) = 7.8t_{ci}$ for the ionization fraction to reach $x = 0.5$. The initial losses are large, owing to both collisional ionization and collisional excitation by the newly liberated electrons and subsequent radiation. An exception is if the pre-shocked gas is pre-ionized. If the shock is strong, pre-ionization (H^+ and He^+) will be achieved, which diminishes the hydrogen Ly α emission. (There will still be cooling from He II Ly α λ 304 and lines from metal ions.) As the gas cools, recombination becomes more efficient. Once the gas reaches 10^4 K, cooling by forbidden lines of metals will occur. The gas will eventually settle down at $T_1 \approx 5000$ – 8000 K, the temperature of the stable WNM phase (see Heiles & Troland 2003; Kanekar et al. 2003; Patra et al. 2018; Murray et al. 2018).

Ignoring “metals”, the mean particle mass is $\mu = m_H(1 + 4y)/(1 + y + x_0)$. The shock velocity and μ determine the post-shock temperature, T_s through Equation 12. Recall that, in our simplified model, the losses from the shocked nebula are only those associated with hydrogen (line radiation, ionization, free-bound, and free-free). In particular, while we include helium in computing the reduced mass, we do not include losses due to helium. In short, we treat helium as a silent and inactive partner. The energy per H-nucleus and associated electron is $E_0 = qk_B T_s(1 + x_0)$. The end state is when hydrogen has largely recombined and thus the energy per H-atom is $E_1 = qk_B T_1$.

For our fiducial temperature of 10^5 K, we have $E_0 \approx [12.9, 21.5](1 + x_0)$ eV energy per H atom for $q = 3/2, 5/2$. Thus, on simple grounds, we can see that low-velocity shocks will not significantly affect the ionization of the incoming particles. More precise radiative shock models show that fast shocks, $v_s > 110$ km s $^{-1}$, can pre-ionize (H^+ , He^+) the incoming medium (Shull & McKee 1979; Raymond 1979; Dopita & Sutherland 1996).

Example runs are shown in Figures 8 and 9. In addition to the run of physical quantities (T , x , n_H) we also plot the total number of recombinations per H nucleus,

$$N_r = \int \frac{1}{n_H} n_H^2 x^2 \alpha_B(T) dt,$$

and the total number of collisions per atom

$$N_c = \int n_H x(1 - x) \sum_{k=1}^{14} q_k(T) dt.$$

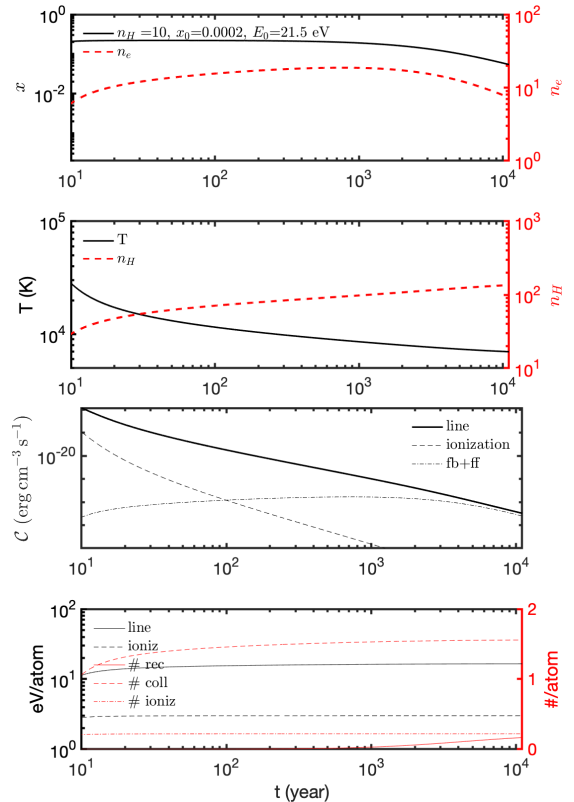


Figure 8. Run of temperature and density of a pure hydrogen plasma suddenly heated to 10^5 K and subsequently cooling down via an isobaric process. The hydrogen density, n_H and ionization, x_0 at $t = 0$ are given in the legend in the top-most panel.

7. CONCLUSION & PROSPECTS

Low velocity shocks with velocities near 70 km s $^{-1}$ abound in our Galaxy. Some descend from higher velocity shocks (e.g., supernova remnants) while others start at low velocity (e.g., stellar bow shocks, high velocity cloud shocks). These shocks do not have strong precursor ionization fronts, and as such the post-shocked gas is partially neutral. Such shocks cool primarily through Ly α , two-photon continuum, H α , and metal emission lines. Ly α is the brightest line, although resonant scattering traps usually traps these photons within the plasma, resulting in absorption by dust grains. H α is weak but has the great advantage of being observable from the ground.

Two-photon continuum emission is about 50% of Ly α emission (see Figure 4). It is several times brighter than H α , even when one compares photon fluxes rather than energy fluxes. Fortunately, two-photon emission can be observed with space-based observatories. Furthermore, the two-photon continuum has a distinct FUV/NUV ratio. In fact, *GALEX* FUV and NUV imagery has led to the recent discovery of large middle-aged supernova

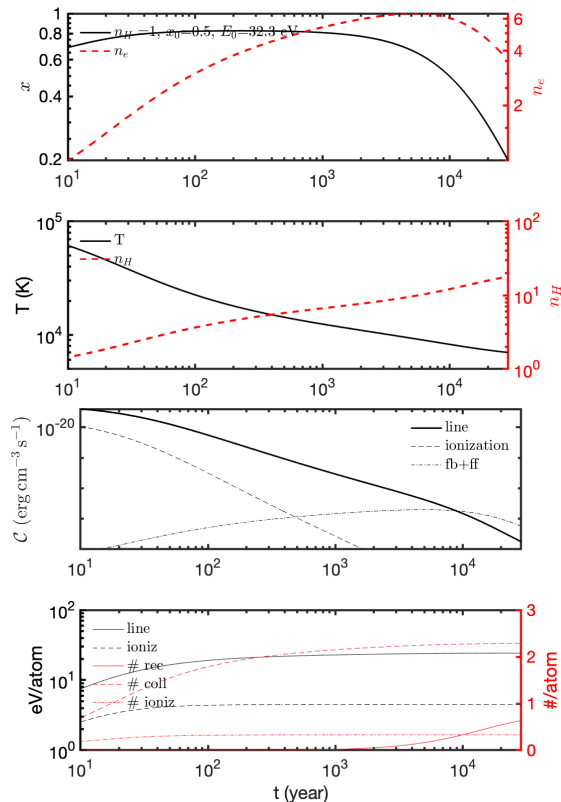


Figure 9. See caption to Figure 8.

remnants (Fesen et al. 2021) and exotic shocked stellar bow shocks with angular scales of hundreds of degrees (Bracco et al. 2020). The Ultraviolet Explorer (UVEX) is a NASA Explorer mission currently under development (Kulkarni et al. 2021). Amongst other goals, UVEX aims to undertake FUV and NUV imaging of the entire sky with higher sensitivity and finer spatial resolution, relative to *GALEX*. The aforementioned successes with *GALEX* imagery show great promise of identifying and studying low velocity shocks in a future all-sky survey with UVEX.

With this motivation, and using the best available atomic physics data and atomic calculations, we computed the collisional and cooling coefficients for warm hydrogen ($T \lesssim 10^5$ K). The primary application of our results is in computing two-photon continuum from bow

shocks and old supernova remnants. We allow for pre-ionization by keeping the ionization fraction of the pre-shocked gas as a free parameter that can be set to values computed from more sophisticated shock models (*ibid*; Dopita & Sutherland 1996). Our expectation is that the accurate H-cooling developed here can be incorporated into time-dependent models (e.g., Gnat & Sternberg 2007).

For completeness, we discuss two-photon emission from photoionized gas (e.g., H II regions, the Warm Ionized Medium). Draine (2011; Table 14.2) provides the recombination coefficient to the 2s level, α_{2s} and the recombination coefficient for H α emission. From this we find ratios

$$\frac{\alpha_{2s}}{\alpha_B} \approx 0.328T_4^{0.115}, \quad \frac{\alpha_{H\alpha}}{\alpha_B} \approx 0.450T_4^{-0.11}. \quad (16)$$

Thus, at typical temperatures of photoionized gas, recombination process result in similar diffuse emission for two-photon continuum and H α . However, while H α emission is concentrated in a narrow line, the two-photon continuum is distributed over the FUV band. Compensating for this effect, the FUV sky is incredibly dark relative to the optical band (see Kulkarni 2022 for detailed analysis of the FUV background).

In the Galactic plane and at low latitudes, two-photon emission will be attenuated by dust in the intervening neutral ISM and contaminated by reflected light from dust grains. In practice, this means that the use of two-photon continuum as a diagnostic will be restricted to high Galactic latitudes and will require careful modeling of reflected light. However, the early success with *GALEX* promises rich returns from the all-sky survey in both the FUV and NUV planned with UVEX.

ACKNOWLEDGMENTS

We thank Nikolaus Zen Prusinski, California Institute of Technology, for help with CHIANTI, a collaborative project involving George Mason University, the University of Michigan (USA), University of Cambridge (UK) and NASA Goddard Space Flight Center (USA).

REFERENCES

- Anderson, H., Ballance, C. P., Badnell, N. R., & Summers, H. P. 2000, *Journal of Physics B Atomic Molecular Physics*, 33, 1255, doi: [10.1088/0953-4075/33/6/311](https://doi.org/10.1088/0953-4075/33/6/311)
- . 2002, *Journal of Physics B Atomic Molecular Physics*, 35, 1613, doi: [10.1088/0953-4075/35/6/701](https://doi.org/10.1088/0953-4075/35/6/701)
- Anguiano, B., Majewski, S. R., Hayes, C. R., et al. 2020, *AJ*, 160, 43, doi: [10.3847/1538-3881/ab9813](https://doi.org/10.3847/1538-3881/ab9813)
- Black, J. H. 1981, *MNRAS*, 197, 553, doi: [10.1093/mnras/197.3.553](https://doi.org/10.1093/mnras/197.3.553)
- Bracco, A., Benjamin, R. A., Alves, M. I. R., et al. 2020, *A&A*, 636, L8, doi: [10.1051/0004-6361/202037975](https://doi.org/10.1051/0004-6361/202037975)

- Chluba, J., & Sunyaev, R. A. 2008, *A&A*, 480, 629, doi: [10.1051/0004-6361:20077921](https://doi.org/10.1051/0004-6361:20077921)
- Dalgarno, A., & McCray, R. A. 1972, *ARA&A*, 10, 375, doi: [10.1146/annurev.aa.10.090172.002111](https://doi.org/10.1146/annurev.aa.10.090172.002111)
- Del Zanna, G., Dere, K. P., Young, P. R., & Landi, E. 2021, *ApJ*, 909, 38, doi: [10.3847/1538-4357/abd8ce](https://doi.org/10.3847/1538-4357/abd8ce)
- Dere, K. P., Landi, E., Mason, H. E., Monsignori Fossi, B. C., & Young, P. R. 1997, *A&AS*, 125, 149, doi: [10.1051/aas:1997368](https://doi.org/10.1051/aas:1997368)
- Dopita, M. A., & Sutherland, R. S. 1996, *ApJS*, 102, 161, doi: [10.1086/192255](https://doi.org/10.1086/192255)
- Draine, B. T. 2011, *Physics of the Interstellar and Intergalactic Medium* (Princeton University Press)
- Draine, B. T., & Salpeter, E. E. 1978, *Nature*, 271, 730, doi: [10.1038/271730a0](https://doi.org/10.1038/271730a0)
- Drake, G. W. F. 1986, *PhRvA*, 34, 2871, doi: [10.1103/PhysRevA.34.2871](https://doi.org/10.1103/PhysRevA.34.2871)
- Fesen, R. A., Drechsler, M., Weil, K. E., et al. 2021, *ApJ*, 920, 90, doi: [10.3847/1538-4357/ac0ada](https://doi.org/10.3847/1538-4357/ac0ada)
- Frisch, P. C., Redfield, S., & Slavin, J. D. 2011, *ARA&A*, 49, 237, doi: [10.1146/annurev-astro-081710-102613](https://doi.org/10.1146/annurev-astro-081710-102613)
- Ghavamian, P., Laming, J. M., & Rakowski, C. E. 2007, *ApJL*, 654, L69, doi: [10.1086/510740](https://doi.org/10.1086/510740)
- Gnat, O., & Sternberg, A. 2007, *ApJS*, 168, 213, doi: [10.1086/509786](https://doi.org/10.1086/509786)
- Gould, R. J., & Thakur, R. K. 1970, *Annals of Physics*, 61, 351, doi: [10.1016/0003-4916\(70\)90289-7](https://doi.org/10.1016/0003-4916(70)90289-7)
- Gry, C., & Jenkins, E. B. 2014, *A&A*, 567, A58, doi: [10.1051/0004-6361/201323342](https://doi.org/10.1051/0004-6361/201323342)
- Heiles, C., & Troland, T. H. 2003, *ApJ*, 586, 1067, doi: [10.1086/367828](https://doi.org/10.1086/367828)
- Hummer, D. G. 1994, *MNRAS*, 268, 109, doi: [10.1093/mnras/268.1.109](https://doi.org/10.1093/mnras/268.1.109)
- Jura, M., & Dalgarno, A. 1972, *ApJ*, 174, 365, doi: [10.1086/151495](https://doi.org/10.1086/151495)
- Kafatos, M. 1973, *ApJ*, 182, 433, doi: [10.1086/152151](https://doi.org/10.1086/152151)
- Kanekar, N., Subrahmanyam, R., Chengalur, J. N., & Safouris, V. 2003, *MNRAS*, 346, L57, doi: [10.1111/j.1365-2966.2003.07333.x](https://doi.org/10.1111/j.1365-2966.2003.07333.x)
- Kim, C.-G., Kim, W.-T., & Ostriker, E. C. 2008, *ApJ*, 681, 1148, doi: [10.1086/588752](https://doi.org/10.1086/588752)
- Kulkarni, S. R. 2022, *PASP*, 134, 084302, doi: [10.1088/1538-3873/ac689e](https://doi.org/10.1088/1538-3873/ac689e)
- Kulkarni, S. R., Harrison, F. A., Grefenstette, B. W., et al. 2021, arXiv e-prints, arXiv:2111.15608, doi: [10.48550/arXiv.2111.15608](https://doi.org/10.48550/arXiv.2111.15608)
- Laming, J. M., Raymond, J. C., McLaughlin, B. M., & Blair, W. P. 1996, *ApJ*, 472, 267, doi: [10.1086/178061](https://doi.org/10.1086/178061)
- Lotz, W. 1967, *ApJS*, 14, 207, doi: [10.1086/190154](https://doi.org/10.1086/190154)
- McComas, D. J., Alexashov, D., Bzowski, M., et al. 2012, *Science*, 336, 1291, doi: [10.1126/science.1221054](https://doi.org/10.1126/science.1221054)
- Murray, C. E., Stanimirović, S., Goss, W. M., et al. 2018, *ApJS*, 238, 14, doi: [10.3847/1538-4365/aad81a](https://doi.org/10.3847/1538-4365/aad81a)
- O'Connell, R. W. 1987, *AJ*, 94, 876, doi: [10.1086/114522](https://doi.org/10.1086/114522)
- Patra, N. N., Kanekar, N., Chengalur, J. N., & Roy, N. 2018, *MNRAS*, 479, L7, doi: [10.1093/mnrasl/sly087](https://doi.org/10.1093/mnrasl/sly087)
- Planck Collaboration, Aghanim, N., Akrami, Y., et al. 2020, *A&A*, 641, A6, doi: [10.1051/0004-6361/201833910](https://doi.org/10.1051/0004-6361/201833910)
- Raymond, J. C. 1979, *ApJS*, 39, 1, doi: [10.1086/190562](https://doi.org/10.1086/190562)
- Scholz, T. T., & Walters, H. R. J. 1991, *ApJ*, 380, 302, doi: [10.1086/170587](https://doi.org/10.1086/170587)
- Scholz, T. T., Walters, H. R. J., Burke, P. J., & Scott, M. P. 1990, *MNRAS*, 242, 692, doi: [10.1093/mnras/242.4.692](https://doi.org/10.1093/mnras/242.4.692)
- Shull, J. M., & McKee, C. F. 1979, *ApJ*, 227, 131, doi: [10.1086/156712](https://doi.org/10.1086/156712)
- Shull, J. M., & Silk, J. 1979, *ApJ*, 234, 427, doi: [10.1086/157511](https://doi.org/10.1086/157511)
- Spitzer, L. 1978, *Physical processes in the interstellar medium* (Wiley), doi: [10.1002/9783527617722](https://doi.org/10.1002/9783527617722)
- Vallée, J. P. 2017, *The Astronomical Review*, 13, 113, doi: [10.1080/21672857.2017.1379459](https://doi.org/10.1080/21672857.2017.1379459)
- Zank, G. P., Heerikhuisen, J., Wood, B. E., et al. 2013, *ApJ*, 763, 20, doi: [10.1088/0004-637X/763/1/20](https://doi.org/10.1088/0004-637X/763/1/20)

APPENDIX

A. COMPARISON TO OTHER COOLING MODELS

In this section we compare our cooling curve, $\Lambda_{\text{HI}}(T)$, discussed in §5, to some notable published curves.

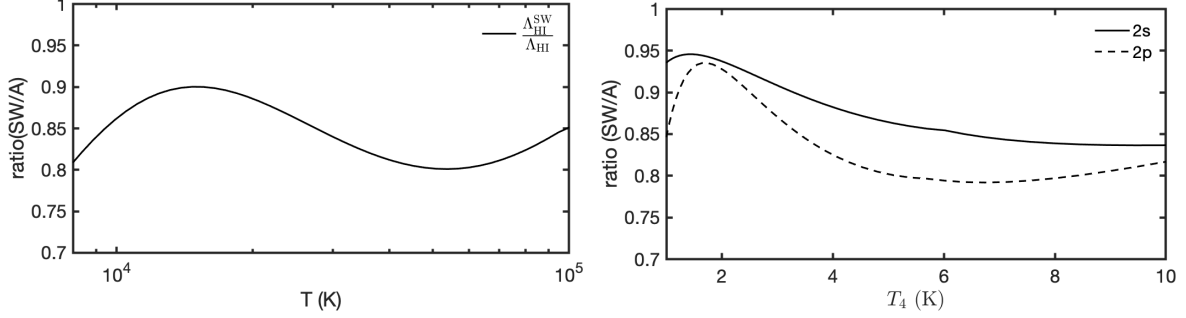


Figure 10. (Left) Comparison of hydrogen line-cooling rate from Scholz & Walters (1991), $\Lambda_{\text{HI}}^{\text{SW}}(T)$ given in Equation A1, with our $\Lambda_{\text{HI}}(T)$ (Equation 3). The ordinate is the ratio $\Lambda_{\text{HI}}^{\text{SW}}(T)/\Lambda_{\text{HI}}(T)$. (Right). Comparison of the collisional line excitation coefficients of $1s \rightarrow 2s$ and $1s \rightarrow 2p$ transitions between Scholz & Walters (1991) (“SW”; see Equation A2, and the corresponding equation of Anderson et al. (2002) (“A”). The ordinate is the ratio $q_{1s \rightarrow f}$ from Scholz & Walters (1991) to that of Anderson et al. (2002).

A.1. Scholz & Walters (1991)

Scholz & Walters (1991) provide collisional ionization coefficient (Equation 8) and total cooling (line and ionization energy losses) coefficients. The latter is given by the following polynomial model:

$$\Lambda_{\text{H}}^{\text{SW}}(T) = 10^{-20} \times \exp\left(\sum_{i=0}^5 d_i y^i - \frac{T_{12}}{T}\right) \text{ erg cm}^3 \text{ s}^{-1} \quad (\text{A1})$$

where $T_{12} = (3/4)T_R$ with $k_B T_R = I_{\text{H}}$ and $y = \ln T$. We subtracted losses to ionization, $\Lambda_{ci} = k_{ci} I_{\text{H}}$, to obtain $\Lambda_{\text{HI}}^{\text{S}}(T)$. In Figure 10 we compare our $\Lambda_{\text{HI}}(T)$ (Equation 3) to $\Lambda_{\text{HI}}^{\text{S}}(T)$. The Scholz-Walters curve is systematically lower by 15%. After correction for this scale factor, the two curves agree to within $\pm 5\%$. Separately, Scholz & Walters (1991) codified the collisional coefficients for excitation from the ($1s$) ground state of hydrogen to $f = 2s$ and $2p$ levels

$$q_{1s \rightarrow f}(T) = \Gamma_{1s \rightarrow f}(T) \exp(-T_{12}/T) \quad (\text{A2})$$

where $\Gamma_{1s \rightarrow f}$ is formulated as

$$\Gamma_{1s \rightarrow f}(T) = \exp\left(\sum_{i=0}^5 b_i y^i\right) \text{ cm}^3 \text{ s}^{-1} .$$

In Figure 10 we compare these two coefficients with our own coefficients (§3). As with the total line emission cooling, the $2s$ and $2p$ collisional rate coefficients are discrepant by the same scale factor.

A.2. Spitzer (1978)

A classical formula for the volumetric cooling rate of hydrogen plasma is given in Spitzer (1978), $\mathcal{C} = n_e n_{\text{H}} \Lambda_{\text{Spitzer}}$, where

$$\Lambda_{\text{Spitzer}}(T) = 7.3 \times 10^{-19} \exp(-T_{12}/T) \text{ erg cm}^3 \text{ s}^{-1}. \quad (\text{A3})$$

We are aware that our cooling coefficient formulation expresses the line cooling rate per unit volume as $n_e n_{\text{HI}} \Lambda_{\text{HI}}$. However, there is little difference between our formulation and Spitzer’s formulation when the ionization fraction is

small. This fit to $\Lambda_{\text{HI}}(T)$ was claimed to be accurate to 3% over the range 4,000 K to 12,000 K. This formula does not include losses from collisional ionization. Spitzer's fit was actually made to H I cooling rates taken from Table 2 of Dalgarno & McCray (1972) which were based on H I excitation cross sections assembled by Gould & Thakur (1970) from theoretical calculations in the 1960s. Those atomic calculations are superseded by more recent work used in this paper (Anderson et al. 2002). In the left panel of Figure 11 we display the ratio of our cooling curves, Λ_{HI} and $\Lambda_{\text{H}} = \Lambda_{\text{HI}} + k_{ci}I_{\text{H}}$ to the cooling rate of Spitzer (Equation A3). Our fit is tuned to be accurate over the range 10^4 K to 10^5 K. Even bearing this in mind, it appears that Spitzer's formula over-estimates line cooling at temperatures above 10^4 K by about 25%.

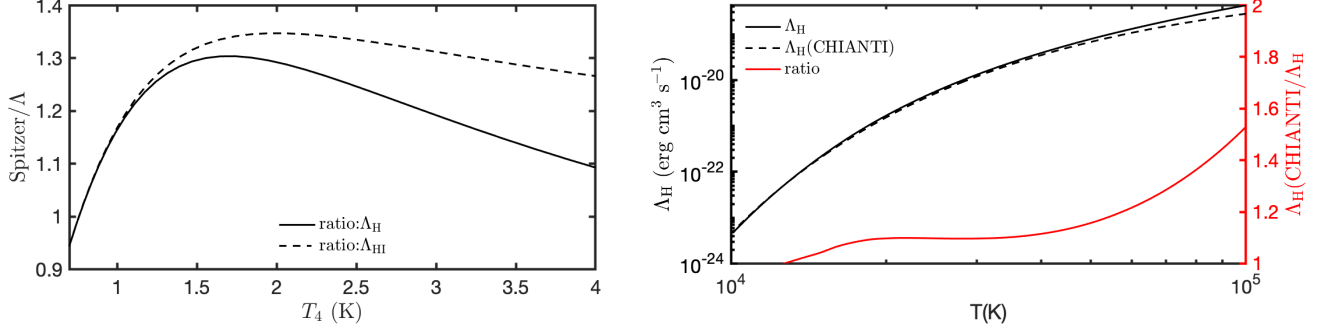


Figure 11. (Left). The ratio of Spitzer's H-line cooling function to our computations of Λ_{HI} (line cooling) and Λ_{H} (including collisional ionization) as a function of temperature. (Right). Comparison of the total cooling curve (line and ionization losses) between our cooling curve and that from CHIANTI.

A.3. Collisional Ionization Equilibrium: CHIANTI

We conclude this section by briefly discussing hydrogen plasma which is in collisional ionization equilibrium (CIE; electron ionization balanced by radiative recombination). The volumetric cooling rate in CIE is given by $\mathcal{C} = x_{\text{eq}}(1 - x_{\text{eq}})n_{\text{H}}^2\Lambda_{\text{CIE}}$ where x_{eq} is given by Equation 14. It is mainly dominated by line cooling. CHIANTI (Dere et al. 1997; Del Zanna et al. 2021) is a major resource for astronomers working on collisionally excited gas, especially hot plasma which are in CIE. CHIANTI returns x_{eq} and cooling function $\mathcal{C} \equiv n_e n_{\text{H}} \Gamma$ (under assumption of case A). Thus, $\Gamma = (1 - x_{\text{eq}})\Lambda_{\text{H}}$.

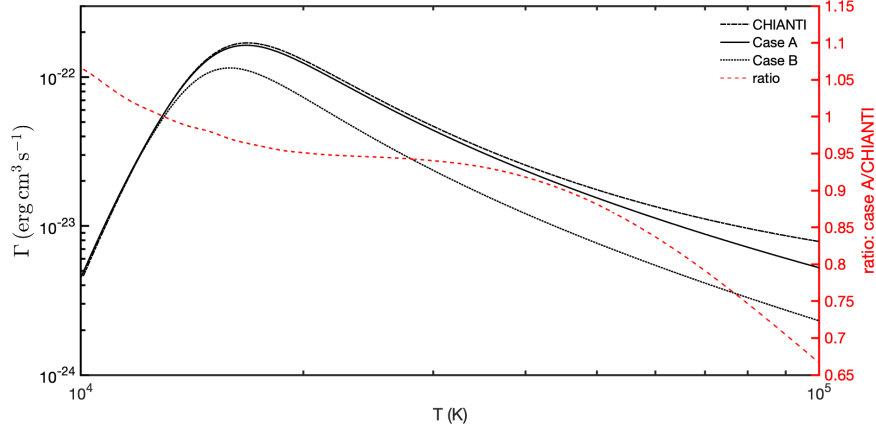


Figure 12. (Left): The run of Γ as obtained from CHIANTI and the calculations reported here (case A, CIE) with temperature T . Here, the Γ_{CIE} is defined as follows: $\mathcal{C} = n_e n_{\text{H}} \Gamma_{\text{CIE}}$ where it is understood that \mathcal{C} and n_e reflect CIE conditions. (Right): The ratio of Γ (this work) to that reported from CHIANTI.

The run of Γ from with temperature is displayed in Figure 12. It is evident that Γ from CHIANTI is brighter relative to the calculations reported here at higher temperatures. There is a small difference As can be seen from Figure 13 our x_{eq} agrees with that used in CHIANTI for $T > 2 \times 10^4$ K.

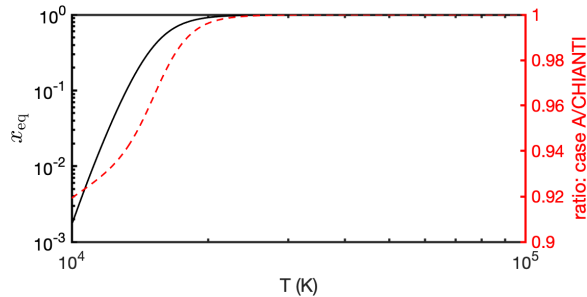


Figure 13. (Left) The run of x_{eq} under CIE conditions as a function of temperature, T . (Right) The ratio of x_{eq} (this paper) to that provided by CHIANTI.

B. LOSSES DUE TO RECOMBINATION, FREE-FREE EMISSION AND IONIZATION

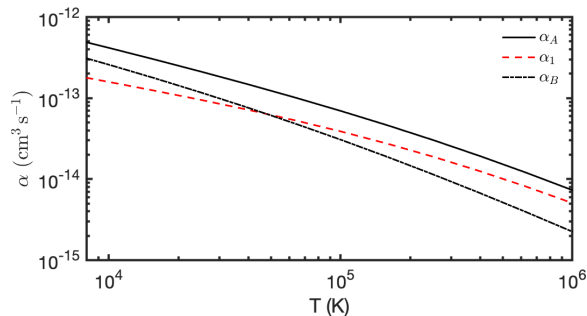


Figure 14. Run of H-recombination coefficients (from Hummer 1994).

Standard textbooks (e.g., [Draine 2011](#)) provide fitting formulae for hydrogen (recombination, free-bound losses) tuned for study of H II regions. Here, we present fitting formula in the temperature range interest to this paper: 10^4 K to 10^5 K. Our starting point is [Hummer \(1994\)](#) who, over an impressive range of 10 K to 10^7 K, present recombinations rate coefficients, α_i where $i = 1$ (recombination to $n = 1$) and $i = A, B$ for case A and case B; see [Figure 14](#).

Separately, [Hummer \(1994\)](#) also tabulate the kinetic energy loss due to recombination and free-free emission. In [Figure 15](#) we plot the mean kinetic energy, $\langle E_{\text{rr}} \rangle$ versus T . Note that $\langle E_{\text{rr}} \rangle = f_{\text{rr}} k_B T$. The resulting fits are presented in [Table 7](#) and are accurate to one percent.

For free-free emission rate coefficient, Λ_{ff} we use Equation 10.12 of [Draine \(2011\)](#) and from that derive $f_{\text{ff}}(T)$ (see §5 for definition of f_{ff}). The values of $f_{\text{rf}} = f_{\text{rr}} + f_{\text{ff}}$ for case A and case B are displayed in [Figure 15](#) (left panel). We assume a simple linear relation and obtain the following fits for f_{rf} :

$$f_{\text{rf}} = 0.71 + 0.0154T_4 \text{ (case A)}, \quad f_{\text{rf}} = 1.10 + 0.0898T_4 \text{ (case B)} .$$

We conclude this section with a discussion of collisional ionization. The energy of the electron, E , upon collision goes into ionizing the atom and imparting kinetic energy to the newly liberated electron. We use the low-energy approximation (Equation 7) for the collisional cross-section, $\sigma_{ci} \propto [1 - (E/I_H)]$ (valid for $I_H \leq E \leq 3I_H$) to find a mean kinetic energy following ionization,

$$\langle E_k \rangle = \langle E - I_H \rangle = \frac{\int_{I_H}^{\infty} \sigma_{ci}(E) v f_E(E - I_H) dE}{k_{ci}(T)} \approx 2k_B T .$$

This formula becomes inaccurate at high temperature ($kT \gtrsim 3I_H$) where the adopted fit to σ_{ci} breaks down (σ_{ci} peaks and then falls off as $\ln E/E$). The energy $\langle E_k \rangle$ is shared between the colliding electron and the ionized electron. This energy is not a loss since it is returned to the thermal pool. However, over time, the ionized electron will draw $qk_B T$ energy ($q = 3/2$ in isochoric framework and $q = 5/2$ in isobaric framework) from the thermal pool. This is a genuine loss (see the discussion following [Equation 15](#)).

Table 7. Fits to α and f

qty	A	n	b
α_1	1.58×10^{-13}	-0.518	-0.039
α_A	4.16×10^{-13}	-0.708	-0.030
α_B	2.58×10^{-13}	-0.822	-0.045
f_{rr}^A	0.784	-0.042	-0.020
f_{rr}^B	0.672	-0.109	-0.021
f_{rf}^A	1.09	0.035	0.019
f_{rf}^B	1.17	0.087	0.061

NOTE—“qty” is fitted to the model of the form $\text{qty} = AT_4^{m+b\ln T_4}$ where the temperature range is $5 \times 10^3 \text{ K} < T < 2 \times 10^5 \text{ K}$; here, $T_4 = T/(10^4 \text{ K})$. See text for definition of subscripts. The superscripts stand for case A or case B. The unit for α is $\text{cm}^3 \text{ s}^{-1}$ while that for f is dimensionless. The fits are accurate to 1% over the temperature range of interest.

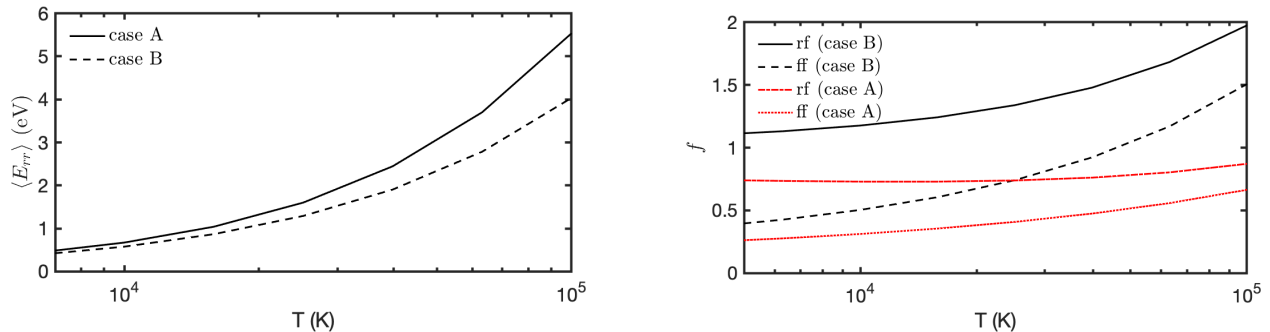


Figure 15. (Left): The run of the average kinetic energy of the recombining electron, $\langle E_{rr} \rangle$, as a function of temperature. (Right): The run of f as a function of temperature (T). The superscripts denote case A or case B. The subscript is “rr” (free-bound radiative recombination), “ff” (free-free emission), and $f_{rf} = f_{ff} + f_{rr}$.

C. TWO SOLUTIONS TO RECOMBINATION-IONIZATION EQUATION

Equation 13 can be written as

$$\frac{dx}{dt} = \frac{x}{\tau_{ci}} - \frac{x^2}{\tau_h},$$

where $\tau_h^{-1} = \tau_{ci}^{-1} + \tau_r^{-1}$ is the harmonic mean of the two timescales. The equilibrium value for ionization is obtained by setting the LHS to zero, $x_{eq} = \tau_h/\tau_{ci}$. The above equation can be re-arranged to yield

$$\frac{dx'}{x'[1-x']} = \frac{dt}{\tau_{ci}},$$

where $x' = x/x_{eq}$. This equation can be integrated using the method of partial fractions to yield

$$\ln \left| \frac{x'}{1-x'} \right| = \frac{t}{\tau_{ci}} + \text{const.}$$

At $t = 0$, $x' = x_0/x_{eq} \equiv x'_0$ and thus

$$\frac{t}{\tau_{ci}} = \ln \left| \frac{x'(1-x'_0)}{x'_0(1-x')} \right|.$$

This equation is useful to compute the time-scale to achieve a particular level of ionization. As $t \rightarrow \infty$, $x \rightarrow x_{eq}$, as expected. Alternatively, we apply the transformation, $u = 1/x$:

$$\left[\frac{du}{dt} + \frac{u}{\tau_{ci}} \right] = \frac{1}{\tau_h}.$$

Multiply both sides by $e^{t/\tau_{ci}}$ to obtain

$$\left[e^{t/\tau_{ci}} \frac{du}{dt} + \frac{u}{\tau_{ci}} e^{t/\tau_{ci}} \right] = \frac{1}{\tau_h} e^{t/\tau_{ci}}.$$

Because the LHS is the derivative of $ue^{t/\tau_{ci}}$, the above equation can be readily integrated to yield

$$u(t) = u_0 e^{-t/\tau_{ci}} + u_{eq} \left[1 - e^{-t/\tau_{ci}} \right]$$

where $u(t=0) = u_0 = x_0^{-1}$ and $u_{eq} = x_{eq}^{-1}$. As $t \rightarrow \infty$, as expected, $u^{-1} \rightarrow x_{eq}$.